

Spatial Relationship Between Twist in Active Region Magnetic Fields and Solar Flares

Michael Hahn¹, Stacy Gaard², Patricia Jibben³, Richard C. Canfield³

and

Dibyendu Nandy³

ABSTRACT

Twisted magnetic field lines in solar active regions constitute stressed flux systems, the reconnection of which can release the stored (excess) magnetic energy in the form of solar flares. Using co-registered photospheric vector magnetograms and chromospheric H α images for 29 flares, we explore the spatial relationship between these flares and the magnetic topology of the active regions in which they occur. We find two dominant trends. First, flares are preferentially initiated in sub-regions that have an high gradient in twist. Second, flare initiation occurs close to chirality inversion lines (which separate regions with twist of opposite handedness). Our results demonstrate that magnetic helicity, as manifested in the twist parameter, plays an important role in magnetic reconnection and solar flaring activity.

Subject headings: MHD — Sun: magnetic fields — sunspots — Sun: flares

1. Introduction

Solar active region magnetic fields are thought to be created by a dynamo mechanism deep within the Sun. They buoyantly rise through the convection zone to form ARs (see e.g., Nandy & Choudhuri 2001). The magnetic field lines of ARs break out to the outer solar atmosphere forming magnetic loops that connect the sub-photospheric regions to higher layers (Longcope & Welsch 2000 and references therein). The general theoretical understanding is that the sub-photospheric convective motions tangle, twist and shear the footpoints of these

¹Department of Physics, Carnegie Mellon University, Pittsburgh, PA 15213, USA.

²Department of Geography and Meteorology, Valparaiso University, Valparaiso, IN 46383, USA.

³Department of Physics, Montana State University, Bozeman, MT 59717, USA.

magnetic loops, which leads to topological complexities and builds up a stressed flux system (and excess energy). Subsequent magnetic reconnection results in the release of energy in the form of flares (Hess 1964; Svestka 1976; Priest & Forbes 2000). Various observational studies have explored the connection between such photospheric magnetic flux systems and solar flares, supporting the hypothesis that solar flares are driven by the reconnection of magnetic fields. Observational evidence of magnetic-reconnection-related relaxation of twisted magnetic fields has been found prior to eruptive flares (Canfield & Reardon 1998; Des Jardins & Canfield 2003) and in H α surges (Jibben & Canfield 2004).

It has long been known that flares tend to occur along magnetic polarity inversion lines (between oppositely directed vertical magnetic fields) and often where the magnetic field lines are highly sheared, with the transverse field directed nearly parallel to the polarity inversion line (Svestka 1976; Hagyard et al. 1984; Sawyer, Warwick & Dennett 1986). Sheared or twisted (non-potential) magnetic flux systems carry large-scale currents along their axis and in earlier work it has been conjectured that the dissipation of these currents in the chromosphere or corona is associated with flares (Alfven & Carlqvist 1967). However, detailed observations find that flares do not necessarily (spatially) coincide with the sub-regions of strongest vertical current within ARs (Canfield et al. 1993; de La Beaujardiere, Canfield & Leka 1993; Metcalf et al. 1994; Li et al. 1997). Subsequent observations point out that topological properties of sheared or twisted AR flux systems, e.g., chirality, may influence solar activity. Canfield, Pevtsov & McClymont (1996) showed that active regions preferentially connect across the equator with others of the same chirality, creating trans-equatorial loops. Jibben & Canfield (2004) found that chromospheric surges preferentially occur along chirality inversion lines.

The purpose of this observational study is to elucidate and further explore the role of pre-flare magnetic field topology in the flaring activity of AR flux systems. Towards that goal, we explore here the spatial relationship between the twist (a component of magnetic helicity) in pre-flare AR flux systems and solar flares. We combine and co-register data from two different instruments, one for flare imaging, the other for magnetic field twist measurements, with procedural details given in Section 2. Our results are presented in Section 3; we find that flares tend to originate in sub-regions (of an AR flux system) that have an high gradient in twist and that the flares tend to lie close to, or over, chirality inversion lines. We discuss the implications of our results and conclude in Section 4.

2. Observations

Since this study involves relating solar flares to magnetic field topology, we used two different instruments for our observations. The Mees Solar Observatory Imaging CCD Spectrograph (MCCD; Penn et al. 1991) was used for flare imaging, while the Haleakala Stokes Polarimeter (HSP; Mickey 1985) was used for the magnetic field observations. We used feature recognition to co-register the two datasets (Canfield et al. 1993).

2.1. Instruments

The MCCD data constitutes $H\alpha$ spectroheliograms in the spectral range $H\alpha \pm 10 \text{ \AA}$ obtained by scanning the solar image from a 25 cm Coudé coronagraph telescope across a spectrograph slit. Pixels in the spectral dimension and one spatial dimension (along the spectrograph slit, terrestrial North-South) are sampled simultaneously, while the other spatial dimension is built up sequentially. It takes about 20 s to complete a scan. The resultant data have $2.3'' \text{ pixel}^{-1}$ spatial and $\sim 0.37 \text{ \AA pixel}^{-1}$ spectral resolution, with a field of view ranging from $108'' \times 117''$ to $230'' \times 290''$ depending on the observing sequence.

The HSP makes simultaneous observations of the Stokes profiles I, Q, U and V of the spectral lines Fe I $\lambda 6301.5$ and $\lambda 6302.5 \text{ \AA}$. Pixels in the spectral dimension are sampled simultaneously, while the two spatial dimensions are built up sequentially, with a typical scan time of an hour. Vector magnetograms are obtained from these Stokes profiles using the Unno-fitting scheme (Unno 1956; Rachkovsky 1962) of Skumanich & Lites (1987), at either of two different pixel spacings of $2.8''$ or $5.6''$. This determines the magnetic field parallel (longitudinal field, B_l) and transverse (B_{trans}) to the line-of-sight and the azimuth ϕ of the transverse field at each raster point. Faraday rotation and magnetic filling factor effects are corrected for and the 180° azimuthal ambiguity in B_{trans} is resolved and all the three components of the vector magnetic field (B_x , B_y and B_z in the heliographic coordinate system) are calculated using the techniques described in Canfield et al. (1993).

2.2. Data Analysis

Our goal in this study is to examine what role the pre-flare magnetic topology (related to the twist in the magnetic field lines) may play in flaring activity. This necessitates the co-spatial comparison of the magnetic field configuration (prior to flaring events) to the subsequent flare images. This was implemented in the following way. We first searched for MCCD flare data that corresponded to flaring events documented by the GOES satellites. We

identify the MCCD image comprising the earliest detection of the flare-related brightening as our start-of-flare image (say, at time t_0), making sure that the brightening was consistently present and getting enhanced in the subsequent frames and could therefore be positively identified as a flare related brightening. We used a difference image for this start-of-flare image, subtracting a pre-flare MCCD image, and integrating over a 2.2 \AA range immediately blueward of $H\alpha$ line center to get the flare difference image (henceforth called start-of-flare image) for use in this study. This resulted in a value of $H\alpha$ flare (enhancement) intensity $I_{H\alpha}(x, y)$ at each pixel (x, y) of the $H\alpha$ image. The use of the blue wing, in contrast to line center or red wing, maximizes the sensitivity to impulsive-phase heating of the chromosphere (Wang & Qiu 2002), rather than the dynamic response (Gayley & Canfield, 1991).

For each of the flaring events, associated with any given AR, when corresponding MCCD observations near the start time of the flare (t_0) could be found, we searched for available HSP vector magnetogram observations within 12 hours prior to the MCCD start-of-flare image (i.e., within 12 hours prior to t_0). It is known that the topological twist parameter α evolves with a characteristic timescale of about 27 hours (Pevtsov, Canfield & Metcalf 1994). This conservative 12 hour cut-off makes sure that the comparison of the pre-flare magnetic field topology to the flare images is physically meaningful. This search culminated in 29 such pre-flare HSP vector magnetogram and MCCD flare image combinations, most within a 6 hour time-frame.

The next step of spatially co-registering the images was achieved by aligning the HSP vector magnetograms to the MCCD images, using a standard routine that performs a least squares fit to points corresponding to features (typically small sunspots or components of complex sunspots) flagged by the user in both the images. White light continuum images having the same dimensions as the observed vector magnetic fields and $H\alpha$ emission, from the HSP and MCCD instruments, respectively, were used for this purpose. This technique results in the stretching and (or) re-orientation of one of the images. Also, since the resolution of the HSP magnetograms is coarser, interpolation was necessary to co-register them with the MCCD images (taking into account the different resolution of the two instruments). This alignment routine for the white light images results in a conversion matrix that could be subsequently used for co-registering the HSP vector magnetogram (and any of its topological derivatives) to the MCCD $H\alpha$ flare images. Visual comparison between the original images and the co-registered images confirmed that the above procedure was working properly. The residuals of the fit show that the accuracy of this method is about $3''$ or better (Canfield et al., 1993).

The end result of this data reduction procedure was 29 co-spatial HSP vector magnetogram and MCCD $H\alpha$ flare image pairs having the same spatial dimensions, and the same

size and number of pixels along both the spatial dimensions, corresponding to 29 different flare events spanning the years 1991 - 2001, which we used for subsequent analysis.

We are interested in comparing properties of the magnetic field topology involving the twist, to the start-of-flare images. The twist in the magnetic field lines of a solar AR is a component of the magnetic helicity associated with the AR flux system (writhe being the other component). In practice, observational estimates of the parameter α associated with the force-free field equation

$$\nabla \times \mathbf{B} = \alpha(x, y)\mathbf{B} \quad (1)$$

are taken to be a measure of the twist associated with a AR flux system (for a straight and uniformly twisted cylindrical flux tube, the parameter α can be shown to be proportional to the twist per unit length). Although the parameter α appears in the force-free field equation, the determination of the quantity does not explicitly assume the observed field to be force-free. Once the three components of the heliographic magnetic field (B_x , B_y and B_z) are determined from the vector magnetogram, the vertical current density $J_z(x, y)$ can be calculated through the relation:

$$J_z(x, y) = \frac{1}{\mu_0} \left[\frac{dB_y}{dx} - \frac{dB_x}{dy} \right]. \quad (2)$$

From this one can calculate the vertical component of the twist parameter

$$\alpha_z(x, y) = \mu_0 \frac{J_z(x, y)}{B_z(x, y)} \quad (3)$$

where B_z is the vertical magnetic field and $\mu_0 = 4\pi \times 10^{-3} \text{ G m A}^{-1}$, is the permeability of free space. In this paper, we refer to this observationally measured quantity $\alpha_z(x, y)$ simply as the twist parameter α of magnetic field lines. The 1σ noise level in the magnetograms is less than 100 G for the transverse field and 10 G for the longitudinal field. For this study we calculate α_z only for pixels for which $|B_{trans}| > 300 \text{ G}$ (i.e., with a cut-off above the 3σ level) thereby ensuring a high degree of confidence in the distribution of α_z that we obtain (Pevtsov, Canfield, & Metcalf 1994). Thus the parameter $\alpha_z(x, y)$ is calculated at each pixel in the high magnetic field region ($> 300 \text{ G}$) of the vector magnetogram. A map of the $\alpha_z(x, y)$ pattern over the spatial scale of the AR, therefore, indicates how the twist varies over this flux system (see e.g., Figure 1).

3. Results

We are now ready to compare the co-spatial pre-flare magnetic field topology (HSP vector magnetograms) and the start-of-flare images (MCCD blue-wing $\text{H}\alpha$ intensity maps)

to explore the role of magnetic field topology in flare initiation. In the previous section, we described how we calculate the distribution of our basic parameter – the twist $\alpha_z(x, y)$ – over the spatial scale of ARs. Our analysis in this section focuses on how certain spatial derivatives of such $\alpha_z(x, y)$ maps relate to solar flaring activity. First, we explore the relationship between the distance to the chirality (handedness of twist or sign of α) inversion line and flaring. Second, we study the relationship between the spatial gradient in twist and flaring activity. Both of these studies yield significant results, which are discussed below.

3.1. Co-registered Magnetic Field Maps and Flaring Images

The calculation for the distance to the chirality inversion line was done by examining the $\alpha_z(x, y)$ maps and assigning a value of “zero” distance to all pixels in a given HSP vector magnetogram that had a neighboring pixel with a value of twist $\alpha_z(x, y)$ of opposite sign. The positions of all the “zero” distance pixels were stored and the distances between these “zero” pixels and all other pixels were found. The distance to the inversion line for any pixel (i, j) was defined as the distance $d(i, j)_0$ to the nearest of the inversion pixels with prior assigned values of “zero”. Co-registration of the resultant $d(x, y)_0$ distribution over the whole AR vector magnetogram with the H α flare image was done for subsequent statistical analysis and checks were performed on “test” magnetograms to ensure the accuracy of this procedure. This procedure was repeated for all the 29 ARs in our dataset.

For illustrative purposes, we present in Figure 1 contours of $\alpha_z(x, y)$ – determined from a HSP vector magnetogram of AR 6982 – overlaid on the corresponding start-of-flare MCCD H α blue-wing image. In this figure it is seen that the initial flare-related intensity enhancements lie close to twist inversion lines [i.e., lines separating oppositely directed twist $\alpha_z(x, y)$].

For calculating the spatial gradient in the twist distribution $\alpha_z(x, y)$ from the HSP vector magnetograms we utilized the following scheme. For the pixel of interest, lets say, (i, j) , we determined the spatial gradient of twist with respect to each of its neighboring pixel (taking into account the different spacings along the vertical, horizontal and diagonal directions) and took the average value (over the number of neighbors) of the amplitude of the gradient and assigned it as the representative gradient of twist, $\text{grad}[\alpha_z(i, j)]$, for this particular pixel. This process was repeated over the whole magnetogram, thereby constructing a map of $\text{grad}[\alpha_z(x, y)]$. Note that some pixels, which had values of $|B_{trans}| < 300$ G, would have been excluded from the analysis because of the cut-off we used to ensure that our α_z maps are relatively error-free. Keeping this in mind we calculated the gradient for only those pixels where values of α_z were defined and which had at least 3 neighbors with defined values of α_z (for pixels which did not satisfy this condition the gradient was set to zero). The distribution

$\text{grad}[\alpha_z(x, y)]$ was then spatially co-registered with the corresponding MCCD H α flare image (using the method described in Section 2.2), thereby enabling the spatial correlation analysis of the gradient of twist with flare initiation sites. Visual comparisons of the contour maps of the original distribution of $\alpha_z(x, y)$ and $\text{grad}[\alpha_z(x, y)]$ to the co-registered maps were performed to make sure that the gradient was being properly calculated and represented in the final co-spatial maps and this procedure was repeated for all the 29 ARs.

Figure 2 depicts the end result of this procedure, a co-spatial contour map of the gradient in twist $\text{grad}[\alpha_z(x, y)]$ – determined from a HSP vector magnetogram of AR 6919 – overlaid on the corresponding start-of-flare MCCD H α blue-wing image. We see in this figure that the region of brightest emission at the flare initiation time spatially coincides with the region of strongest gradient in twist.

3.2. Statistical Analysis

Many of the 29 different magnetic field topology and H α flare image pairs in our dataset showed the trend that can be ascertained from a visual inspection of the co-spatial images such as those depicted in Figure 1 and Figure 2. Nevertheless, some did not and certainly a robust quantitative analysis was in order to establish any trends (or lack thereof) in the data. We performed a statistical (Spearman’s Rank correlation) analysis of the data using diverse methods for quantifying the trends and checking for their consistency. We discuss them here.

To begin with, we looked at the pixel by pixel (spatial) correlation of both the distance to the inversion line $d(x, y)_0$ and gradient in twist $\text{grad}[\alpha_z(x, y)]$ with the H α flare intensity $I_{H\alpha}(x, y)$, separately, for each of the 29 flare events. All negative pixels found in the MCCD H α intensity maps (in the final difference images) were excluded, as were all pixels in which values of $d(x, y)_0$ and $\text{grad}[\alpha_z(x, y)]$ could not be computed (due to the cut-off used in B_{trans} ; see earlier discussion). For this particular analysis of each flare event, we took 8 MCCD frames (the first corresponding to the start-of-flare image at t_0 , and each subsequent one following at intervals of 20 s, thus spanning about 2-3 minutes at the beginning of the flare) and compared all of the 8 frames to the HSP pre-flare magnetic topology. This multi-frame analysis was done in order to be sure that the result stayed consistent over the eight MCCD frames taken about the flare-start-time and we were not observing some transient event that looked like a flare only in the first frame (at t_0). Any correlation (for each of the 8 frames for a given AR) was deemed significant if the significance of the correlation was $\geq 95\%$. Subsequently, we conservatively defined the correlation for a particular AR-flaring image combination (across the 29 different AR-flaring events) to be “compelling” only if

the correlations were consistently either positive or negative over at least 7 of those 8 HSP magnetic field topology and MCCD flare image subsets for that AR; otherwise the correlation was deemed to be unclear.

With the above methodology, in the 29 different pre-flare magnetic field topology of ARs and H α flare image pairs that comprise our total sample, we found that 13 ARs showed a (pixel by pixel) negative correlation between the distance to the inversion line $d(x, y)_0$ and H α flare intensity $I_{H\alpha}(x, y)$, 4 ARs showed a positive correlation and in 12 ARs the correlation was unclear. In the twist gradient study, 14 of the ARs showed a positive (pixel by pixel) correlation between the gradient in twist $\text{grad}[\alpha_z(x, y)]$ and H α flare intensity $I_{H\alpha}(x, y)$, 6 ARs showed a negative correlation and in 9 ARs the correlation was unclear. We point out here that amongst the 14 ARs which showed a positive correlation between $\text{grad}[\alpha_z(x, y)]$ and $I_{H\alpha}(x, y)$, 5 ARs *also* showed a negative correlation between $d(x, y)_0$ and $I_{H\alpha}(x, y)$. It is also noteworthy that none of the 29 ARs showed both a negative correlation between $\text{grad}[\alpha_z(x, y)]$ and $I_{H\alpha}(x, y)$ and a positive correlation between $d(x, y)_0$ and $I_{H\alpha}(x, y)$. Keeping our already conservative approach in mind, we take these results as an indication that flares tend to be initiated in regions of high twist gradient and that the flare initiation regions tend to lie close to chirality inversion lines.

Figure 3 is a scatter plot of the correlations coefficients between $\text{grad}[\alpha_z(x, y)]$ and $I_{H\alpha}(x, y)$ and $d(x, y)_0$ and $I_{H\alpha}(x, y)$. Only those co-registered frames which showed significant correlations ($\geq 95\%$) have been plotted here. The dashed line shows a linear fit, which should be taken in the spirit of just indicating the trend and not necessarily to imply that one expects a linear correlation. Most of the points are in the upper-left hand quadrant, which indicates that the data conforms to the two predominant trends – regions of high twist gradient correlates positively with H α flare-intensity and flare-intensity correlates negatively with distance to the chirality inversion line (i.e., regions of high flare-intensity lie close to chirality inversion lines).

To quantify the statistical significance of these two tendencies we combined the data from all 29 different flare events, building up two different datasets; one cumulative dataset for the distance to the inversion line $d(x, y)_0$ and H α flare intensity $I_{H\alpha}(x, y)$ study; the second cumulative dataset for the twist gradient $\text{grad}[\alpha_z(x, y)]$ and H α flare intensity $I_{H\alpha}(x, y)$ study. A pixel by pixel (spatial) correlation of this combined dataset between $d(x, y)_0$ and $I_{H\alpha}(x, y)$ yielded a negative Spearman’s rank correlation coefficient of -0.05 with a significance of 99.99% (see second row in Table 1), while a similar correlation between $\text{grad}[\alpha_z(x, y)]$ and $I_{H\alpha}(x, y)$ yielded a positive Spearman’s rank correlation coefficient of 0.08 with a significance of 99.99% (see second row in Table 2). Note that the Spearman’s correlation coefficient is based on a distribution of ranks and therefore not limited to only linear trends (Press et al.

1986). Although the correlation coefficients are small, the high significance levels indicate that the trends are real. This quantitative statistical approach thus confirms the trends of our earlier analysis, namely that flares tend to originate in regions of high twist gradient and lie close to chirality inversion lines.

Finally, we check for statistical consistency in the trends with respect to relative errors in the data. The most significant source of instrumental error in our data lies in the noise level for the transverse component of the magnetic field B_{trans} (about 100 G) measured by the HSP. We have already taken a 3σ cut-off in B_{trans} (300 G) to ensure accuracy in our magnetic field maps. However, to check for the robustness of our data analysis procedure it is necessary to analyze how the statistical inferences vary due to varying amounts of error in the data. For this purpose, we repeat the earlier combined correlation study (in which we used a cutoff in $B_{trans} = 300$ G), now with different cutoffs for B_{trans} , namely 250 G (which introduces more noise and therefore amplifies errors in the subsequent data analysis) and 350 G (which reduces noise and errors in the subsequent data analysis). The results are summarized in Table 1 and Table 2, for $d(x, y)_0$ versus $I_{H\alpha}(x, y)$ correlations and $\text{grad}[\alpha_z(x, y)]$ versus $I_{H\alpha}(x, y)$ correlations, respectively. It is found that when the amount of error in the data is systematically reduced, (starting from B_{trans} cutoffs of 250 G, through 300 G, to 350 G), the correlations between the relevant quantities, systematically increase towards the predominant trend. This leads us to conclude that the inferred trends in the data are consistent and robust.

4. Discussions

Our aim in this study was to explore the relationship between pre-flare magnetic field topology and flaring activity, with special emphasis on where the flare initiation was taking place. Our analysis, through the co-registration of the data from two disparate instruments, one for the vector magnetic field (HSP magnetograms) and the other for flare imaging ($H\alpha$ images from MCCD), has uncovered two dominant trends. First, flares tend to be initiated in regions of high gradient in twist and second, flare initiation occurs close to chirality inversion lines that separate regions of oppositely directed twist. Since our analysis was confined to sub-regions (pixels) with $|B_{trans}| > 300$ G (to ensure our α -maps were relatively error free), it is prudent to note that these results apply within regions of high magnetic field. Our findings are of obvious interest, first, as a potential pointer to precursors for flares and perhaps more importantly in its implications for theoretical aspects of flaring activity.

Earlier observational studies have shown that flares tend to lie across magnetic polarity inversion lines separating oppositely directed magnetic fields (reviewed by Sawyer, Warwick,

& Dennett 1986), implicating magnetic reconnection as the basis for flares. It has also been reported that flares tend to occur preferentially over sheared polarity inversion lines (Hagyard et al. 1984), indicating that stressed non-potential flux systems may play a role in flaring activity through reconnection, subsequent release of the excess energy and relaxation of the shear.

Twisted magnetic fields in the outer solar atmosphere with non-zero values of α are examples of such stressed flux systems and if the twist is unequally distributed across the flux system it constitutes a non-linear force-free magnetic field configuration. In the context of such a stressed magnetized low- β (ratio of gas to magnetic pressure) plasma system in the solar atmosphere, Taylor’s hypothesis (Woltjer 1958; Taylor 1974, 1986) of plasma relaxation implies that the system relaxes (via magnetic reconnection) to a lower energy state such that the final magnetic field configuration is a linear force-free field with the twist equally distributed across the whole flux system (see also Heyvaerts & Priest 1984). Earlier, Nandy et al. (2003) had found that solar ARs that released more energy through flaring activity also tended to show a higher decrease in the statistical variance of twist α (not to be confused with the spatial gradient) over the AR flux system, thus indicating a relaxation towards a linear force-free state. Other theoretical studies indicate that the evolution of twist through magnetic reconnection may be a hyper-diffusive mechanism, i.e., a relaxation process *driven* by the non-uniformity in the twist distribution itself (Bellan 2000; Diamond & Malkov 2003). The results of the present paper support this theoretical idea and complement the earlier observation of Nandy et al. (2003) showing that a high gradient (or disparity) in twist values over the spatial scale of the flux system promotes flaring and this flaring activity is initiated over regions of strongest twist gradient and close to chirality inversion lines. Note that regions that lie over chirality inversion lines necessarily have a high value of twist gradient, because the twist changes sign across this line; so in essence, the two main results of our analysis are supplementary.

The participation of M.H. and S.G. in this project was made possible by NSF Research Experience for Undergraduates grant ATM-0243923 to Montana State University. We acknowledge financial support from NASA through Supporting Research and Technology grant NAG5-11873.

REFERENCES

Alfvén, H., & Carlqvist, P. 1967, Sol. Phys., 1, 220

- Bellan, P. M. 2000, *Spheromaks: A Practical Application of Magnetohydrodynamic Dynamics and Plasma Self-Organization* (London; Imperial College Press)
- Canfield, R. C., et al. 1993, *ApJ*, 411, 362
- Canfield, R. C., Pevtsov, A. A., & McClymont, A. N. 1996, in *Magnetic Reconnection in the Solar Atmosphere*, ed. R. D. Bentley, & J. T. Mariska (A.S.P. Conference Series, 111), 341
- Canfield, R. C. & Reardon, K. P. 1998, *Sol. Phys.*, 182, 145
- de La Beaujardiere, J.-F., Canfield, R. C., & Leka, K. D. 1993, *ApJ*, 411, 378
- Des Jardins, A. C., & Canfield, R. C. 2003, *ApJ*, 598, 678
- Diamond, P. H., & Malkov, M. 2003, *Phys. Plasmas*, 10, 2322
- Gayley, K. G., & Canfield, R. C. 1991, *ApJ*, 380, 660
- Hagyard, M. J., Teuber, D., West, E. A., & Smith, J. B. 1984, *Sol. Phys.*, 91, 115
- Hess, H. E. 1964, in *The Physics of Solar Flares*, ed. H. E. Hess (Proceedings of the AAS-NASA Symposium; Washington, DC)
- Heyvaerts, J., & Priest, E. R. 1984, *A&A*, 137, 63
- Jibben, P., & Canfield, R. C. 2004, *ApJ*, 610, 1127
- Li, J., et al. 1997, *ApJ*, 482, 490
- Longcope, D. W., & Welsch, B. T. 2000, *ApJ*, 545, 1089
- Metcalf, T. R., et al. 1994, *ApJ*, 428, 860
- Mickey, D. L. 1985, *Sol. Phys.*, 97, 223
- Nandy, D., & Choudhuri, A.R. 2001, *ApJ*, 551, 576
- Nandy, D., Hahn, M., Canfield, R. C., & Longcope, D. W. 2003, *ApJ*, 597, L73
- Penn, M. J., Mickey, D. L., Canfield, R. C., & LaBonte, B. J. 1991, *Sol. Phys.*, 135, 163
- Pevtsov, A. A., Canfield, R. C., & Metcalf, T. R. 1994, *ApJ*, 425, L117
- Press, W. H., Teukolsky, S. A., Vetterling, W. T., & Flannery, B. P. 1986, *Numerical Recipes in Fortran 77* (Cambridge; Cambridge University Press)

- Priest, E., & Forbes, T. 2000, *Magnetic Reconnection: MHD Theory and Applications* (Cambridge: Cambridge University Press)
- Rachkovsky, D. N. 1962, *Izv. Krymsk. Astrofiz. Obs.* 27, 148
- Sawyer, C., Warwick, J. W., & Dennett, J. T. 1986, *Solar Flare Prediction* (Colorado: Colorado Associated University Press)
- Skumanich, A., & Lites, B. W. 1987, *ApJ*, 322, 473
- Svestka, Z. 1976, *Solar Flares* (Dordrecht:Reidel)
- Taylor, J. B. 1974, *Phys. Rev. Lett.*, 33, 1139
- Taylor, J. B. 1986, *Rev. Mod. Phys.*, 58, 741
- Unno, W. 1956, *PASJ*, 8, 108
- Wang, H., & Qiu, J. 2002, *ApJ*, 568, 408
- Woltjer, L. 1958, *Proc. Nat. Acad. Sci. (USA)*, 44, 489

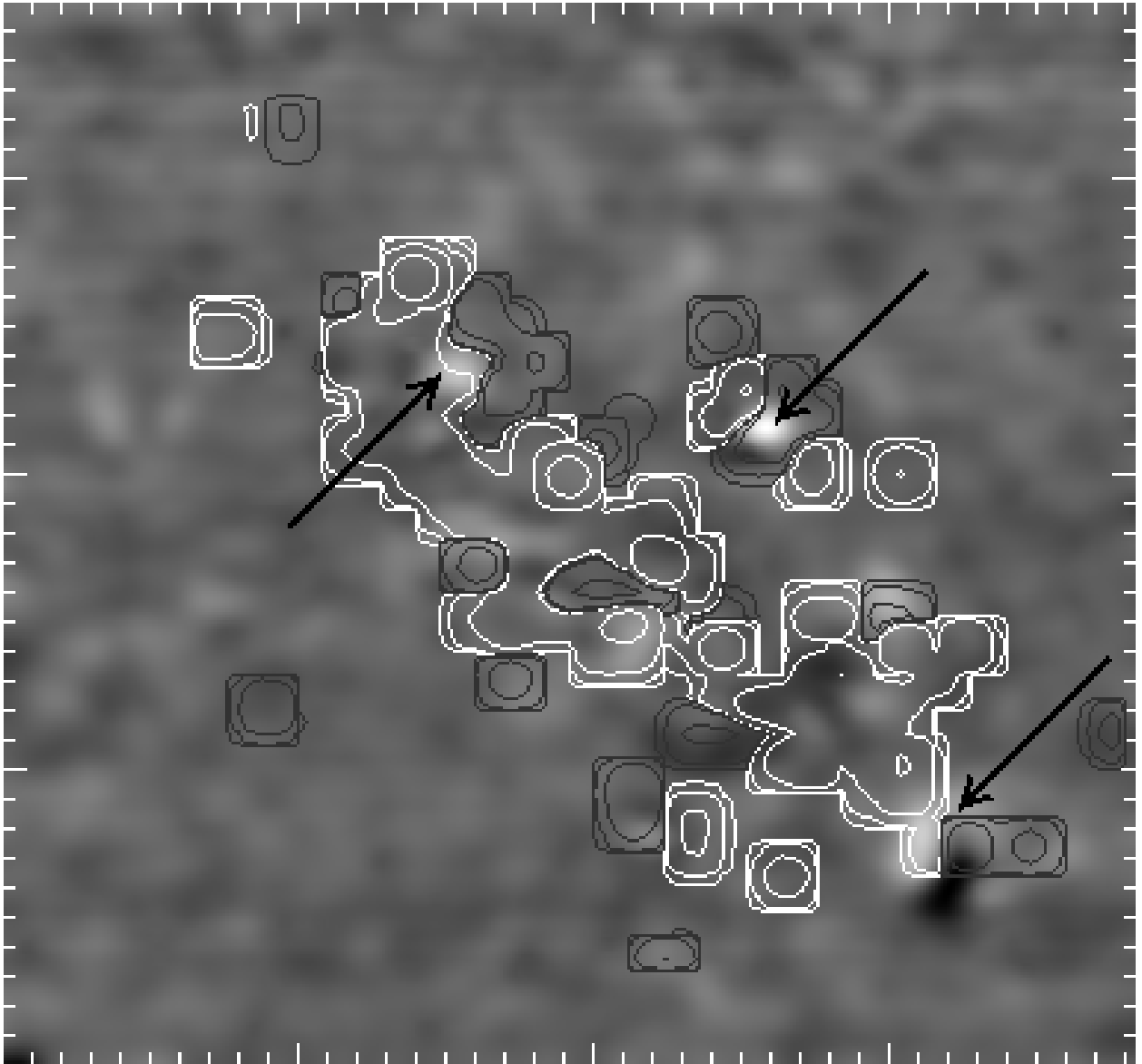


Fig. 1.— A contour map of the twist distribution $\alpha_z(x, y)$ from a pre-flare HSP vector magnetogram of AR 6982 (started at 28 December, 1991 at 18:42 UT) overlaid on the corresponding gray-scale M CCD $H\alpha$ start-of-flare blue-wing intensity image (taken the same day at 21:07:34 UT). The scale of the image is 159.94×148.67 Mm. White contours show regions with positive twist and black contours show regions with negative twist. The black arrows point to regions of strong $H\alpha$ emission associated with the start of the flare, showing them to lie close to chirality inversion lines.

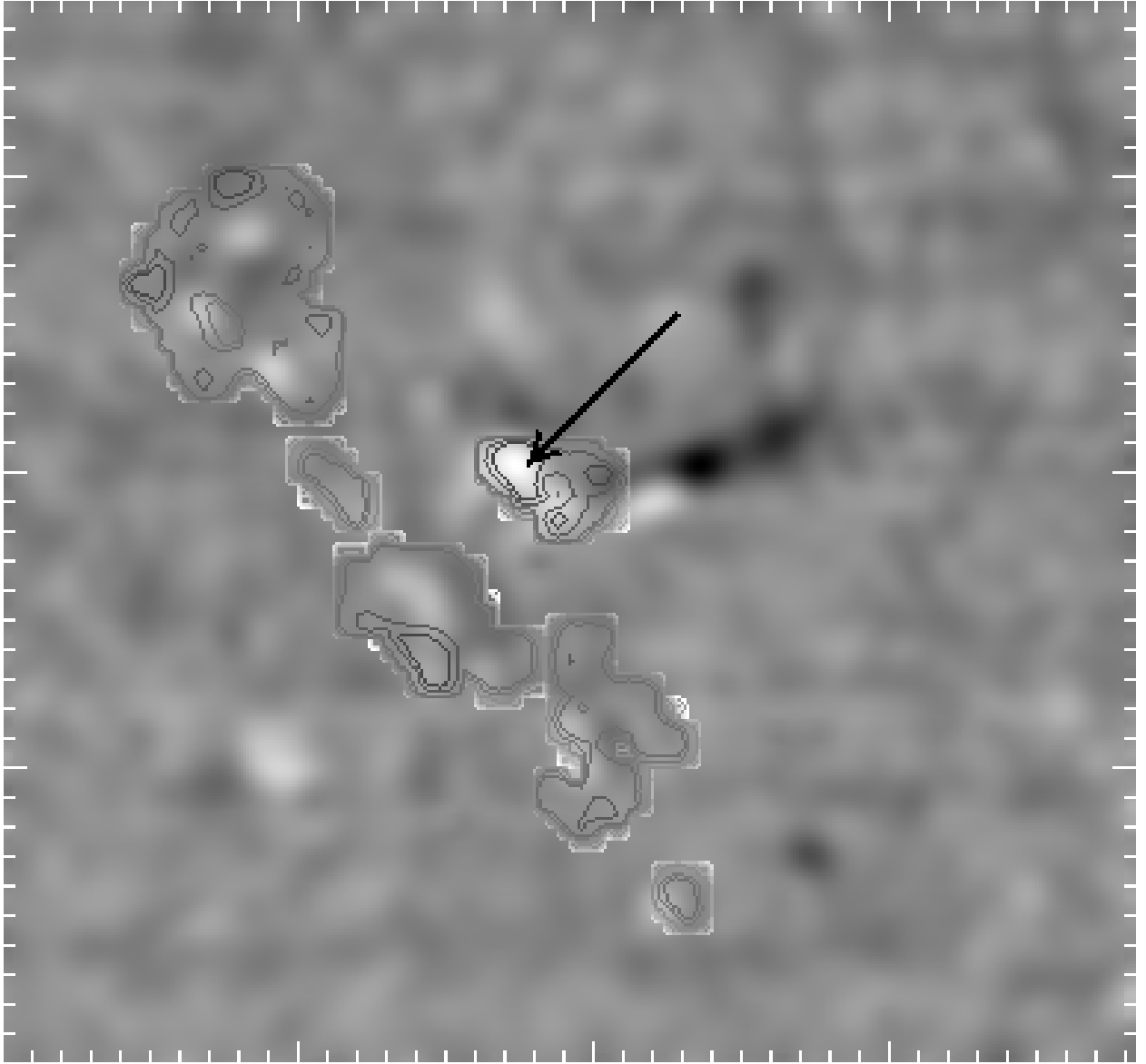


Fig. 2.— Contours of the gradient in twist $\text{grad}[\alpha_z(x, y)]$ from a pre-flare HSP vector magnetogram of AR 6919 (started on 15 November, 1991 at 21:05 UT) overlaid on the corresponding gray-scale MCCD H α start-of-flare blue-wing flare intensity $I_{H\alpha}(x, y)$ image (taken the same day at 22:32:04 UT). The scale of the image is 161×150 Mm. Darker contours denote stronger gradients. The black arrow marks the region of brightest intensity in H α emission showing it to be co-spatial with the strongest gradient in twist.

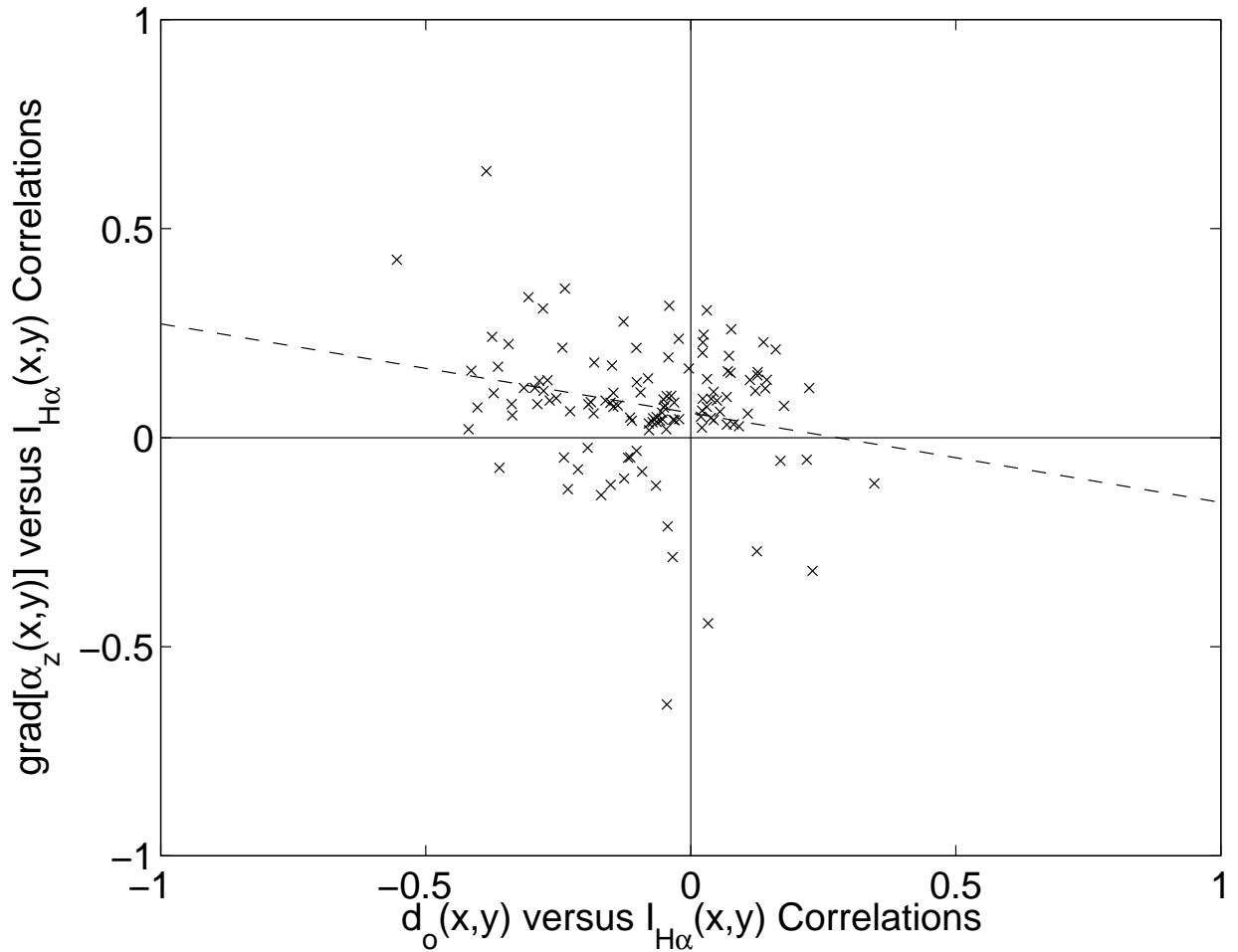


Fig. 3.— A scatter plot of the correlation coefficients of distance to inversion line and flare intensity correlations (x -axis) versus twist gradient and flare-intensity correlations (y -axis). Only significant correlations ($\geq 95\%$) between the co-registered HSP magnetic topology and MCCD H α flare image frames are plotted. The dashed line shows the linear least-squares fit to the data (significance of linear correlation is 98.86%). Most of the points lie in the upper-left quadrant showing the dominant trend.

Table 1. Combined Inversion Line Distance & Flare Intensity Correlations

Cutoff	Correlation Coefficient	Significance
250G	-0.0128	99.99%
300G	-0.0498	99.99%
350G	-0.1260	99.99%

Table 2. Combined Twist Gradient & Flare Intensity Correlations

Cutoff	Correlation Coefficient	Significance
250G	-0.0071	99.99%
300G	0.0841	99.99%
350G	0.1250	99.99%